Optimal HVAC Energy and Regulation Reserve Scheduling in Power Markets

Waleed Aslam, Panagiotis Andrianesis, *Member, IEEE*, and Michael Caramanis, *Senior Member, IEEE*

***Abstract*—This paper considers the optimal scheduling of the hourly energy consumed and regulation reserve capacity offered by a Heating, Ventilation and Air-Conditioning (HVAC) system participating in a day-ahead electricity market. We formulate an Integrated hourly energy and regulation reserve Scheduling and Deployment (ISD) problem that optimizes the hourly costs and benefits resulting from the power consumed, the regulation reserve capacity offered, the occupant thermal comfort utility, and the expected Intra-Hour Costs (IHCs) due to HVAC's imperfect tracking of the regulation signal broadcasted by the Independent System Operator every few seconds. Addition of the IHCs to the objective function is the major innovation of this paper. It enables optimal HVAC scheduling to internalize expected regulation signal tracking error cost traded-off against incremental occupant thermal discomfort that may result from perfect tracking. The cost causation circle closes by noting that a high hourly regulation reserve offer may result in higher expected IHCs by increasing the associated tracking error and the incremental occupant discomfort. The paper's innovation is achieved by (i) estimating an analytic function of the hourly HVAC scheduling decision and state variables that approximates the expected IHCs, and (ii) including this exogenously estimated analytic function in the objective of the hourly ISD optimization problem. Non-convexities introduced to the optimization problem resulting from high fidelity HVAC model and the inclusion of the expected IHCs, are addressed efficiently through piecewise convex relaxations that provide tight optimality bounds. Extensive numerical results are provided to demonstrate the applicability and performance of the proposed approach.**

***Index Terms*—Energy and reserve scheduling, frequency regulation, heating ventilation and air-conditioning (HVAC) systems.**

NOMENCLATURE

Sets and Indices	
t	hour index, (Δt denotes interval duration)
n, k	partition index for $m, \bar{\theta}$ in bilinear term
n, n'	partition indices for m in quadratic term
Input Parameters	
c	specific heat capacity of air
R^b, R^w	thermal resistance (building mass, window)
C, C^b	thermal capacitance (inside air, building mass)
Q	heat transfer due to occupancy and irradiance
θ^a, θ^s	ambient temperature, supply air temperature
δ	valve position
η	coefficient of performance of coil
α	coefficient of fan power consumption
λ^P, λ^R	energy price, regulation reserve price
$\hat{\theta}$	set-point temperature.
Variables	
$decision$	
m	supply air flow rate
r	regulation reserve capacity
$state$	
$\theta, \bar{\theta}$	inside air temperature, average θ
$\theta^b, \bar{\theta}^b$	building mass temperature, average θ^b
$auxiliary$	
ξ	equivalent linear variable for the bilinear term
ζ	equivalent linear variable for the quadratic term
w, u	weights for discretization points
x, y	indicators for interval activation
Functions of Decision and State Variables used for Compact Notation	
$\Delta\theta^c$	air temperature change at the cooling coil
p	HVAC power consumption
p^f, p^c	power consumption (fan, cooling coil)
Q^s	heat exchange between inside air and supply air
$J_{t(m_t, r_t, \theta_{t-1}, \theta^b_{t-1}, \bar{\theta}_t)}$	expected intra-hour cost (IHCs) for hour t

Manuscript received 14 December 2022; revised 1 April 2023; accepted 16 May 2023. Date of publication 23 May 2023; date of current version 19 December 2023. This work was supported in part by the FMJH PGMO-IROE program under Grant 2020-0009, and benefited from the EDF support to this program. Paper no. TSTE-01272-2022. *(Corresponding author: Waleed Aslam)*

Waleed Aslam is with the Systems Engineering Division, Boston University, Boston, MA 02215 USA (e-mail: waslam@bu.edu).

Panagiotis Andrianesis is with the Department of Wind and Energy Systems, Technical University of Denmark, 2800 Kgs. Lyngby, Denmark, also with the Centre for Processes, Renewable Energy and Energy Systems, (PERSEE), Mines Paris, PSL University, 06904 Sophia Antipolis, France, also with the Systems Engineering Division, Boston University, Boston, MA 02215 USA (e-mail: panosa@bu.edu).

Michael Caramanis is with the Department of Mechanical Engineering and the Systems Engineering Division, Boston University, Boston, MA 02215 USA (e-mail: mcaraman@bu.edu).

Color versions of one or more figures in this article are available at https://doi.org/10.1109/TSTE.2023.3279060.

Digital Object Identifier 10.1109/TSTE.2023.3279060

I. INTRODUCTION

THE ever increasing penetration of clean, albeit volatile, renewable power generation is introducing a myriad of challenges to the efficient and secure operation of the electric

grid, calling upon demand to play a significant role. Storage-like and bidirectional regulation reserve capabilities of distributed energy resources including smart thermostats and electric vehicles are coming to the forefront, with Heating, Ventilation and Air-Conditioning (HVAC) systems being particularly relevant due to their load-shifting capabilities in preheating/precooling and their fast bi-directional power consumption response around a nominal value [1], [2], [3], [4], [5], [6].

This work focuses on HVAC systems that present an attractive value proposition for a number of reasons. Firstly, HVACs tend to be an abundant resource; there were about 116 million HVAC units globally in 2018 and their number is expected to rise to 151 million by 2024 [7]. Secondly, they are the largest contributor to building energy consumption but possess unused energy storage-like capabilities due to the associated thermal inertia of air and building structures [8]. Thirdly, they are typically controlled by buildings' Energy Management Systems, whose capabilities can be easily leveraged with minimal impact on occupant comfort.

HVAC systems can regulate their power consumption by modulating the fan/pump speed to control the flow rate of air supplied into the building [9], [10], [11], or the flow rate of water to the chiller [12]. HVAC systems can most efficiently utilize their fans/pumps to track stochastic, albeit energy-neutral, intra-hour regulation reserve signals broadcasted by an Independent System Operator (ISO) [13]. This enables HVAC systems to obtain revenues by offering regulation reserve capacity in the day-ahead market, provided that they do not incur relatively inordinate Intra-Hour Costs (IHCs) during the ISO's deployment of regulation reserve signals [14].

The HVAC scheduling problem is considered in [9], [10], [11], [12], [15], [16], [17], [18] as a Non-Linear Programming (NLP) problem that determines optimal power consumption and regulation reserve capacity trajectories for given day-ahead market energy and reserve prices. However, these works do not model IHCs. They instead impose hard constraints that *either* incur large IHCs by over-committing on the regulation reserve capacity offer, *or*, assure negligible IHCs at the expense of limiting the regulation reserve capacity offer and the associated opportunity for additional revenues. For instance, the hard constraints are determined by considering a confidence-interval-based worst-case weather and regulation signal percentile (e.g., 95-th in [9], 97.5-th in [10], [11]), or an uncertainty set based worst-case in [12], [15], [17]. Indeed, the size of the hourly reserve capacity offered, the HVAC/building state, and the level of the intra-hour regulation signal broadcasted by the ISO, may result in IHCs consisting of regulation signal tracking error penalties and occupant discomfort [19], [20]. Modeling of IHCs and anticipating them when hourly decisions are made, makes this work stand out in the literature.

This paper focuses on optimizing the *hourly* energy consumed and regulation reserve capacity offered by an HVAC system participating in the day-ahead electricity market. Its novelty is the incorporation into the objective function of the *expected IHCs* resulting from the HVAC's obligation to modulate its power consumption during the ISO's deployment of the hourly offered regulation reserve capacity. These IHCs internalize the expected regulation tracking error and incremental occupant discomfort incurred in the HVAC's best effort to follow ISO regulation reserve signals. We formulate an Integrated hourly Scheduling and Deployment (ISD) problem by including into the optimized objective function the IHCs along with the hourly cost of power consumed, the revenue from regulation reserve capacity offered, and the space-conditioning derived occupant discomfort cost. As such, our ISD problem is unique in the optimal HVAC scheduling literature in the context of hourly day-ahead markets. We employ a pre-processor, exogenous to the ISD problem, which draws from and expands work reported in [21] and [22], to estimate the expected IHCs — i.e., the regulation signal tracking error and incremental building occupant discomfort *average cost*, incurred during each hour reflecting the optimal HVAC adaptation to intra-hour regulation signals — as a closed-form analytic function of the hourly decision variables (that refer to HVAC controls and offered regulation reserve capacity) and state variables (that refer to temperature).

Moreover, our ISD problem employs high fidelity models of the HVAC and the building structure's capability to store energy [23] that contain non-convexities. To deal with the non-convexities, in particular a bilinear term and a non-convex quadratic constraint, we relax the complicating terms using piecewise, convex polyhedra. Specifically, we employ a Special Ordered Set (SOS2) based formulation, known as Piecewise Polyhedral Relaxation (PPR) [24], which is known to be tighter compared to standard and piecewise McCormick relaxations while incurring small computational overhead [25]. The resulting formulation is a Mixed Integer Quadratic Program (MIQP) problem, which can be efficiently solved using off-the-shelf solvers, and provides tight bounds on the ISD problem objective. We report numerical results of our formulation on a realistic office building to demonstrate our ISD problem formulation and quantify the tightness of the bounds on the ISD problem objective. We compare with existing approaches and we analyze the impact of different exogenous factors, namely of day-ahead market prices, ambient temperature, and inside air temperature bounds, on the optimal ISD problem decision and state variables.

To summarize, the contribution of this paper is three-fold. First and most important, we formulate an ISD problem, which explicitly accounts for the expected IHCs as a function of hourly HVAC decision and state variables. This allows us to internalize the trade-off captured by the IHCs, between regulation signal tracking error and intra-hour occupant discomfort, into the hourly problem. This is the Second, we present an MIQP relaxation of the (originally NLP) ISD problem, which provides tight bounds for the NLP optimal solution, and we demonstrate its computational performance and tightness through numerical experimentation. To the best of our knowledge this is the first work to provide a computationally efficient method for the ISD problem of a high fidelity HVAC system model. Third, we compare with existing works that employ hard constraints and worst-case-based approaches which are shown to be overly conservative and not adaptive to the frequency regulation signal characteristics, which our approach inherently considers when estimating the expected IHCs.

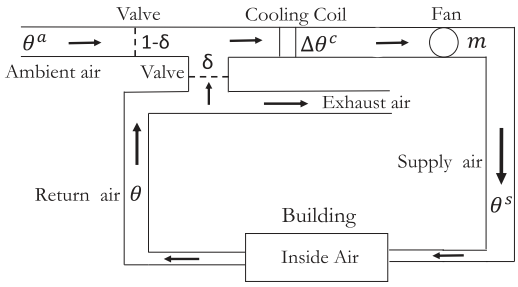

Fig. 1. HVAC model.

The remainder of this paper is organized as follows. Section II presents the HVAC and building model. Section III details the ISD problem NLP formulation and estimation of the expected IHCs. Section IV presents the ISD problem MIQP formulation. Section V describes the Case Study, and Section VI discusses the numerical results. Section VII concludes and suggests the directions for future research.

II. HVAC and Building Model

In this section. we detail the HVAC model (in Section II-A), the building thermal dynamics (in Section II-B), and the hourly decision and state variables (in Section II-C).

A. HVAC Model

We consider a unitary HVAC system as illustrated in Fig. 1 [23], where, for simplicity and without loss of generality, we model the cooling operation. The HVAC mixes the ambient air with the return air from the building in a ratio that is governed by the valve position. This air mixture is then cooled by the cooling coil and circulated inside the building by the fan. The supply air temperature, θ^s, thus satisfies:

$$\theta^s = \delta\,\theta + (1-\delta)\theta^a - \Delta\theta^c, \tag{1}$$

where δ is the valve position, θ is the inside air temperature that is also the return air temperature, θ^a is the ambient temperature, and $\Delta\theta^c$ is the air temperature change at the cooling coil.[1] Typically, the values of the valve position, δ, and supply air temperature, θ^s, are assumed to be fixed [12]. We note that we have dropped the time index for simplicity.

The HVAC total power consumption, p, is given by:

$$p = p^c + p^f, \tag{2}$$

where p^c is the power consumption of the cooling coil, and p^f is the power consumption of the fan.

The power consumption of the cooling coil, p^c, is related to the supply air flow rate, m, and the temperature change, $\Delta\theta^c$, as follows [26]:

$$p^c = m\,\frac{c}{\eta}\,\Delta\theta^c, \tag{3}$$

[1]Considering a heating operation, the supply air temperature θ^s would be larger than the inside air temperature θ_t. Thus, (1) would be written as $\theta^s = \delta\theta + (1-\theta)\theta^a + \Delta\theta^h$, where $\Delta\theta^h$ would be the air temperature change at the heating coil.

where c is the specific heat capacity of the air, and η the coefficient of performance of the coil. Replacing $\Delta\theta^c$ using (1), and rearranging terms, (3) becomes:

$$p^c = \frac{c}{\eta}\delta\,m\,\theta + \frac{c}{\eta}\left[(1-\delta)\theta^a - \theta^s\right] m. \tag{4}$$

Note that the first term in (4) contains a bilinear term $m\,\theta$, whereas the second term depends linearly on m.

The power consumption of the fan, p^f, is described by a quadratic function of the supply air flow rate, m, as follows:

$$p^f = \alpha_1\, m + \alpha_2\, m^2, \tag{5}$$

where α_1 and α_2 are parameters that are fitted using historical fan power data [23]. The fast response of the fan, by adjusting the supply air flow rate, enables the HVAC to modulate its power consumption and deploy regulation reserves [1]. In this work, we consider that regulation reserve follows ISOs' regulation deployment practices, e.g., ISO New England (ISO-NE) and Pennsylvania-Jersey-Maryland (PJM) [13], [27]. Specifically, the regulation reserve capacity r is symmetric — i.e., equal in the up and down directions around the hourly energy consumption — and the regulation signal from the grid operator that is used to modulate power and deploy regulation reserves is energy-neutral over an hour — so that its impact on the HVAC hourly energy consumption is negligible. Hence, the regulation reserve capacity is constrained within the HVAC fan's capability, as follows:

$$p^f - r \geq p^{f-}, \qquad p^f + r \leq p^{f+}, \tag{6}$$

where p^{f-} and p^{f+} represent the minimum and maximum power consumption of the fan, which are determined by the fan capability and bounds on the supply air flow rate, m^- and m^+, respectively. Obviously, the HVAC maximum regulation reserve capability is $(p^{f+} - p^{f-})/2$, when the power consumption of the fan is $p^f = (p^{f+} + p^{f-})/2$.

The HVAC total power consumption (2), using (4) and (5), is given by:

$$p = \frac{c}{\eta}\delta\,m\,\theta + \left[\alpha_1 + \frac{c}{\eta}\left[(1-\delta)\theta^a - \theta^s\right]\right] m + \alpha_2\, m^2. \tag{7}$$

Note that (7) includes a bilinear term $m\,\theta$, and a quadratic dependence on m.

B. Building Thermal Dynamics

The building thermal dynamics are described using the second-order Resistance-Capacitance (RC) model shown in Fig. 2 [28], which represents temperature as a nodal voltage and heat exchange as a current injection. Let R^b, C^b, and θ^b denote the building mass thermal resistance, thermal capacitance, and temperature, respectively, R^w the thermal resistance of windows, and C the thermal capacitance of inside air. Let Q^s denote the heat exchange between inside air and supply air, and Q the heat exchange between inside air and other sources (e.g., irradiance, occupancy).

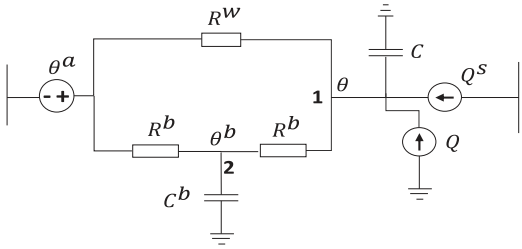

Fig. 2. Resistance-capacitance (RC) model for the building.

Applying Kirchhoff's Current Law at nodes 1 and 2 of Fig. 2, we get the following thermal dynamics:

$$C\dot{\theta} = \frac{\theta^a - \theta}{R^w} + \frac{\theta^b - \theta}{R^b} + Q + Q^s, \tag{8a}$$

$$C^b\dot{\theta^b} = \frac{\theta^a - \theta^b}{R^b} + \frac{\theta - \theta^b}{R^b}, \tag{8b}$$

where $\dot{\theta}$ and $\dot{\theta^b}$ represents the rate of change of the inside air and the building mass temperatures, respectively.

C. Hourly Scheduling Decision and State Variables

Let us now consider the HVAC hourly scheduling. We introduce index t to denote an hour. The HVAC decides the amount of offered regulation reserve capacity, r_t, at each hour t, which is linked to the supply air flow rate m_t. Hence, m_t and r_t are the HVAC *decision variables* for hour t.

The building thermal dynamics determine the *state variables*, i.e., the inside air temperature, θ_t, and the building mass temperature θ_t^b. As can be seen in (8a), these state variables depend on the heat exchange Q_t^s between the inside air and supply air, which in turn is dependent on the decision variable m_t, as follows:

$$Q_t^s = m_t\, c\, (\theta^s - \theta_t). \tag{9}$$

Since the thermal time constant of the building (in the order of 30 hours) is much larger than the hourly granularity, we can accurately approximate the building dynamics using Euler's mid-point method, as follows.

Let $\bar{\theta}_t$ and $\bar{\theta}_t^b$ denote the average hourly temperatures of inside air and building mass, respectively. The inside air temperature dynamics (8a) are approximated by:

$$\theta_t - \theta_{t-1} = \frac{\theta_t^a - \bar{\theta}_t}{R^w C} + \frac{\bar{\theta}_t^b - \bar{\theta}_t}{R^b C} + \frac{Q_t}{C} + m_t \frac{c}{C}(\theta^s - \bar{\theta}_t), \tag{10}$$

where we also replaced Q_t^s using (9). Rearranging the terms in (10), we get:

$$\theta_t - \theta_{t-1} = \frac{c\theta^s}{C} m_t - \frac{c}{C} m_t \bar{\theta}_t - \left(\frac{1}{R^b C} + \frac{1}{R^w C}\right)\bar{\theta}_t + \frac{1}{R^b C}\bar{\theta}_t^b + \frac{Q_t}{C} + \frac{\theta_t^a}{R^w C}. \tag{11}$$

Similarly, the building mass temperature dynamics (8b) are approximated by:

$$\theta_t^b - \theta_{t-1}^b = \frac{1}{R^b C^b}\bar{\theta}_t - \frac{2}{R^b C^b}\bar{\theta}_t^b + \frac{\theta_t^a}{R^b C^b}. \tag{12}$$

Furthermore, the HVAC hourly energy consumption, denoted by p_t (since t refers to one hour), is given by:

$$p_t = \frac{c}{\eta}\,\delta\, m_t\, \bar{\theta}_t + \left[\alpha_1 + \frac{c}{\eta}\,[(1-\delta)\theta^a - \theta^s]\right] m_t + \alpha_2 m_t^2. \tag{13}$$

Notably, increasing participation of storage resources in the provision of frequency regulation is expected to favor the creation of energy-neutral (over an hourly period) regulation signals, *a la* PJM RegD. However, relaxing the energy-neutrality assumption, the deployment of regulation reserve may result in a different temperature at the end of the hour than the anticipated value. Hence, an offset to the energy consumption may be required to be applied in real-time, to counter potential persistence of the regulation signal in either direction. Again, similarly to storage resources, HVACs may be allowed to update their economic basepoints every 5 minutes to adapt to real-time conditions, and correct any differences between the anticipated and actual temperatures.

III. ISD Problem

In this section, we detail the NLP formulation of the ISD problem (in Section III-A), and we detail the estimation of the expected IHCs (in Section III-B).

A. NLP Problem Formulation

Let $t \in \mathcal{T} = \{1, \ldots, 24\}$ denote the set of hours in a day. The NLP formulation is presented below.

1) Objective Function: We reiterate that the ISD problem optimizes the hourly energy consumption and regulation reserve capacity offered by the HVAC in the day-ahead market, while also considering the hourly discomfort cost, and the expected IHCs associated with regulation reserve deployment. The ISD problem objective is:

$$\begin{aligned}&\text{minimize}\{\text{Energy Cost–Regulation Revenue}\\ &\text{+ Discomfort Cost + Total IHCs}\}.\end{aligned} \tag{14}$$

We define each term in (14) below.

$$\text{Energy Cost} = \sum_t \lambda_t^p p_t, \tag{14a}$$

where λ_t^p is the energy price at hour t, and p_t is the HVAC energy consumption at hour t — see (13) — given by

$$p_t = \beta_1 m_t \bar{\theta}_t + \beta_2 m_t + \alpha_2 m_t^2, \quad \forall t, \tag{14b}$$

with $\beta_1 = \frac{c}{\eta}\delta$, and $\beta_2 = \alpha_1 + \frac{c}{\eta}[(1-\delta)\theta_t^a - \theta^s]$.

$$\text{Regulation Revenue} = \sum_t \lambda_t^r r_t, \tag{14c}$$

where λ_t^r is the regulation reserve price at hour t, and r_t is the HVAC offered regulation reserve capacity at hour t.

$$\text{Discomfort Cost} = \sum_t \epsilon_t(\bar{\theta}_t - \hat{\theta}_t)^2, \tag{14d}$$

where ϵ_t is the penalty factor for thermal discomfort at hour t, and $\hat{\theta}_t$ is the HVAC temperature set-point at hour t.

$$\text{Total IHCs} = \sum_t J_t(m_t, r_t, \theta_{t-1}, \theta^b_{t-1}, \bar{\theta}_t), \tag{14e}$$

where, J_t is the "expected IHCs" during hour t. We express J_t as a closed-form analytic function of the hourly decision variables (m_t and r_t) and state variables ($\theta_{t-1}, \theta^b_{t-1}, \bar{\theta}_t$). The expected IHCs, J_t, includes regulation signal tracking error and intra-hour occupant discomfort costs (incremental to the average hourly discomfort cost), which are incurred during regulation reserve deployment when the HVAC discomfort preferences limit regulation signal tracking capabilities. For example, scheduling high regulation reserve capacity will render tracking large regulation signals impossible without compromising occupant discomfort. Therefore, optimal deployment is achieved through the best trade-off between the tracking error and incremental occupant discomfort costs. We essentially capture this trade-off through the use of closed-form J_t acting as a soft constraint penalty.

We note that the decision variables appear in J_t's expression since they impact the intra-hour power modulation (and hence the tracking error), with air flow rate m_t also impacting the intra-hour thermal dynamics (and hence the intra-hour discomfort). The state variables are also included in J_t since they impact the intra-hour building occupant discomfort costs. Specifically, the intra-hour incremental occupant discomfort cost is calculated around the average inside air temperature $\bar{\theta}_t$, whereas the inside air and building mass temperatures at the start of the hour, θ_{t-1} and θ^b_{t-1}, affect the intra-hour temperature dynamics (and thus the intra-hour discomfort costs). This should come as no surprise since J_t is in fact the expected cost-to-go over the hour when the system state at the beginning of the hour is described by θ_{t-1} and θ^b_{t-1}. We detail the estimation of J_t in Section III-B.

2) Constraints: The ISD problem includes thermal dynamics, regulation and bound constraints.

Thermal Dynamic Constraints: The inside air and building mass temperatures are obtained by (11) and (12) as follows:

$$\theta_t = \theta_{t-1} + \gamma_1 m_t + \gamma_2 m_t \bar{\theta}_t + \gamma_3 \bar{\theta}_t + \gamma_4 \bar{\theta}^{\,b}_t + \gamma_{5,t}, \ \forall t, \tag{15}$$

$$\theta^b_t = \theta^b_{t-1} + \gamma_6 \bar{\theta}^b_t + \gamma_7 \bar{\theta}_t + \gamma_{8,t}, \quad \forall t, \tag{16}$$

where $\gamma_1 = c\theta^s/C$, $\gamma_2 = -c/C$, $\gamma_3 = -1/(R^bC) - 1/(R^wC)$, $\gamma_4 = 1/(R^bC)$ and $\gamma_{5,t} = Q_t/C + \theta^a_t/(R^wC)$, $\gamma_6 = -2/(R^bC^b)$, $\gamma_7 = 1/(R^bC^b)$ and $\gamma_{8,t} = \theta^a_t/(R^bC^b)$. For completeness, the average hourly temperatures for the inside air and the building mass are given by:

$$\bar{\theta}_t = \frac{\theta_{t-1} + \theta_t}{2}, \quad \bar{\theta}^b_t = \frac{\theta^b_{t-1} + \theta^b_t}{2}, \quad \forall t. \tag{17}$$

Regulation Constraints: Following (6), and using (5), the regulation reserve capacity, r_t, is constrained as given below:

$$\text{Regulation Up:} \quad \alpha_1 m_t + \alpha_2 m_t^2 - r_t \geq p^{f-}, \quad \forall t, \tag{18}$$

$$\text{Regulation Down:} \quad \alpha_1 m_t + \alpha_2 m_t^2 + r_t \leq p^{f+}, \quad \forall t. \tag{19}$$

Bound Constraints: The fan capability and potential inside air temperature hard limits impose the following bound constraints on m_t and θ_t, respectively:

$$m^- \leq m_t \leq m^+, \quad \theta^-_t \leq \theta_t \leq \theta^+_t, \quad \forall t. \tag{20}$$

3) NLP Problem Summary: The NLP problem formulation is summarized as follows:

$$\textbf{NLP}: \quad \text{minimize } (14), \text{subject to: } (15)\text{–}(20), \tag{21}$$

with variables r_t non-negative, and $m_t, \theta_t, \theta^b_t, \bar{\theta}_t, \bar{\theta}^b_t$ real, $\forall t$.

Note that the NLP problem formulation includes the bilinear term $m_t\bar{\theta}_t$ in the J_t representation of the objective function (14b) and in constraint (15), as well as a non-convex quadratic inequality (18) that includes m_t^2.[2] We treat these complicating terms and constraints with mixed integer linear relaxations next.

B. Estimation of the Expected IHCs.

We employ a pre-processor which is run off line, i.e. prior to the solution of the ISD problem, to estimate parameters of a quadratic approximation of the expected IHCs, J_t, expressed in terms of state and decision variables $(m_t, r_t, \theta_{t-1}, \theta^b_{t-1}, \bar{\theta}_t)$ optimized in the ISD problem. The pre-processor executes the following tasks.

A reasonable seconds time scale regulation reserve deployment controller is used to simulate different l indexed, $l = 1, 2, \ldots, L$, values of expected IHCs, J^l_t, associated with similarly indexed state and decision variable levels $(m^l_t, r^l_t, \theta^l_{t-1}, \theta^{b,l}_{t-1}, \bar{\theta}^l_t)$.

A range of different state and decision variable levels, $l = 1, 2, \ldots, L$, that span the possible hourly state and decision variables which may be encountered in the solution of the ISD problem, is selected and for each of them the average IHCs, J^l_t, are simulated.

We finally estimate the unknown parameters to fit the quadratic function of $(m^l_t, r^l_t, \theta^l_{t-1}, \theta^{b,l}_{t-1}, \bar{\theta}^l_t)$ to the J^l_t values.

The fully specified quadratic, which as noted below is a convex second-degree polynomial (with a single cross-term $m_t\bar{\theta}_t$), is then included in the ISD problem's objective function to integrate expected deployment costs incurred for each contemplated scheduling decision. Estimated parameters for a medium-sized office building are listed in Section V-B.

The pre-processor simulation of the regulation deployment controller and the resulting intra-hour costs depends on intra-hour time scale dynamics that involve a new state variable representing the regulation reserve signal broadcasted by the ISO after 2, 4 or 6 s intervals [13], [27], [30]. In this work, we consider 4 s deployment intervals. Accounting for intra-hour time by τ, the regulation signal state is denoted by $S\tau$ and the control decision representing the modulation in the airflow is denoted by Δm_τ. $S\tau$ is associated with random dynamics

[2] An extension to multi-zone systems, — e.g., [29] considers additional valves in Fig. 1 to control the supply air flow rate to each zone — would involve one bilinear term per zone (with different temperatures per zone), and a quadratic term for the HVAC system. The thermal discomfort cost and IHCs would also be expressed as the sum of the respective costs per zone.

described by a Markov Chain whose transition probabilities are estimated from historical data [21] and can be simulated accordingly. As detailed next, hourly state and decision variables are also associated with the short time scale τ in the intra-hour simulator of IHCs. The simulator of IHCs: (i) starts from the instance l of the HVAC state at the beginning of the hour, (ii) employs Monte Carlo to simulate the regulation signal dynamics to determine $S\tau$, (iii) applies a myopic controller to select a feasible Δm_τ to minimizes current period τ costs by trading off incremental impact on occupant thermal comfort and regulation signal tracking, and as such instantiates a myopic controller (iv) propagates state variables to the next τ period, and (v) sums period costs to arrive to the hourly total, J_t^l.

1) State Variables: Intra-hour simulator state variables include the supply air flow rate m_τ, inside air temperature, θ_τ and building mass temperature θ_τ^b, as well and the regulation signal $S\tau$. The regulation signal is modeled using the approach in [21]. For simplicity of exposition we disregard a second variable used only in the simulation of the underlying Markov chain, focusing instead on $S\tau$ which takes values in the interval [-1, +1] and explicitly impacting each τ period cost. The variables m_τ, θ_τ and θ_τ^b are subject to the bound constraints, same as the ones in the scheduling problem, i.e., (20), which can be enforced as hard or soft constraints. Collectively, all the state variables are denoted as x_τ.

2) Control Variable: The change in air flow rate, Δm_τ, is the control variable which modifies the fan power consumption p_τ^f – see (5) – and allows the tracking of the reference regulation signal. The control variable is limited by the ramp rate and thus allowed to vary within a range $[\Delta m^-, \Delta m^+]$. Note that the cooling coil consumption is not impacted by the control variable since the coil has a slow response and the net change in the control variable over a longer timescale can be considered negligible (due to energy-neutrality assumption).

3) State Dynamics: Dynamics for the air flow rate are given by $m_\tau = m_{\tau-1} + \Delta m_\tau$. Temperature dynamics for θ_τ and θ_τ^b are governed by (15) and (16), where the hourly interval t is replaced by the shorter, seconds scale interval τ. As noted, Regulation signal dynamics are simulated using the procedure described in [21] which employs a second variable associated with increasing or decreasing regulation signal.

4) Fixed Hour-Specific Information: Hour specific Information that is considered to be approximately constant during the simulation of IHCs includes the scheduling variables, i.e., air flow rate m_t, regulation reserve capacity r_t, inside air temperature θ_{t-1}, building mass temperature θ_{t-1}^b, and average inside air temperature $\bar{\theta}_t$. Other information that is intra-hour constant includes the temperature set-point $\hat{\theta}_t$ and allowable temperature range (θ_t^-, θ_t^+), as well as the thermal discomfort penalty factor $\tilde{\epsilon}$ and tracking error penalty factor κ. Ambient temperature θ_τ^a and heat Q_τ for each interval may either be considered deterministic, or stochastic, but in any case independent of ISD problem decisions.

5) Controller Objective: The intra-hour controller's objective is to minimize the cost of regulation reserve deployment tracking error plus the incremental intra-hour thermal discomfort. In particular:

$$\underset{\Delta m_t}{\text{minimize}} \; \underset{x_{\tau+1}|x_\tau}{\mathbb{E}} \Bigg[\sum_\tau \kappa \left(p_t + S_\tau r_t - p_\tau\right)^2 + \tilde{\epsilon} \left(2(\bar{\theta}_t - \hat{\theta}_t)(\theta_\tau - \bar{\theta}_t) + (\theta_\tau - \bar{\theta}_t)^2 \right) \Bigg]. \tag{22}$$

The first term penalizes (by κ) the square of the tracking error during intra-hour period τ, defined as the deviation from the regulation signal specified power consumption above or below the ISD scheduled power consumption $(p_t + S_\tau r_t)$ and the actual power output p_τ. The actual power output is calculated as $p_\tau = p_t^c + p_\tau^f$, with the cooling coil power p_t^c considered fixed and the fan power p_τ^f dependent on the control Δm_τ. The second term penalizes (by $\tilde{\epsilon}$) the incremental thermal discomfort incurred during intra-hour period τ.

Each l indexed instance of the pre-processor's estimation of IHCs has been solved by Monte Carlo simulation of the Regulation reserve signal using the underlying Markov Process and the myopic or greedy heuristic controller described above. It is interesting to note that the myopic controller trades off tracking error cost for thermal comfort, which, when the internal air temperature is way above the maximum comfort set point, will be biased towards positive tracking errors resulting in AC power consumption that exceeds the level scheduled in the hourly ISD problem. The opposite will be true when the internal air temperature is below the max comfort set point. This bias may be welcome in the short term mitigating the impact of unplanned behavior such as open windows that bring hot air into the building, but may it may also interfere with pre-cooling strategies implemented by the ISD problem. Alternative controller designs aiming at discovering optimal or near optimal controllers would have to rely on much more cumbersome stochastic Dynamic Programming formulations of the IHCs pre-processor. This points to interesting future work.

IV. ISD Problem MIQP Formulation

In this section, we describe the relaxations that are used to handle the non-convexities in the NLP formulation of the ISD problem (in Section IV-A), and we summarize the resulting MIQP formulation (in Section IV-B).

A. Mixed Integer Linear Relaxations

Unlike existing works that deal with an NLP formulation of the ISD problem [9], [10], [11], [12], [15], [16], [17], [18], we consider an SOS2-based formulation, known as Piecewise Polyhedral Relaxation (PPR), to relax the bilinear/quadratic terms using piecewise, convex polyhedra [24]. The PPR relaxation provides a piecewise convex hull representation for the feasible region of the NLP problem. It is more powerful than linearization techniques – e.g., a linear approximation of the bilinear / quadratic terms – and provides bounds to the NLP

problem objective. It also offers a tighter relaxation and similar/better computational performance compared to other convex relaxations, such as the standard and piecewise McCormick relaxation [25]. In what follows, we detail the PPR relaxation employed to treat the bilinear term $m_t\bar{\theta}_t$ in the objective function and (15), and the quadratic term m_t^2 of the non-convex quadratic inequality (18).

1) Bilinear Term ($m_t\bar{\theta}_t$): PPR uses a spatial disjunction on the variables and a vertex representation for the bilinear term. It associates a spatial disjunction with each variable, m_t and $\bar{\theta}_t$, by defining a set of discretization points and intervals that partition the domain of the variable. Note that each pair of discretization points from the domain of variables m_t and $\bar{\theta}_t$ represents a vertex. Also note that for a given partition, the convex combination of the bilinear term $m_t\bar{\theta}_t$ values at the vertices represents a convex polyhedron, which is a relaxation of the bilinear term within that partition. Therefore, the convex combination of the bilinear term values at the vertices, considered disjunctively for different domain partitions using special ordered sets, helps characterize the piecewise, convex polyhedral relaxation of the bilinear term.

Let the feasible regions of variables m_t and $\bar{\theta}_t$ be partitioned into N and K intervals using $(N+1)$ and $(K+1)$ discretization points respectively. Let $[\mu_n, \mu_{n+1}]$ and $[\phi_k, \phi_{k+1}]$ denote the discretization values associated with n-th and k-th intervals of variables m_t and $\bar{\theta}_t$ respectively. Let $w_{t,n,k}$ denote a (non-negative) weight associated with vertex (n, k), with

$$\sum_{n=1}^{N+1}\sum_{k=1}^{K+1} w_{t,n,k} = 1, \quad \forall t, \tag{23}$$

so that the domains of m_t and $\bar{\theta}_t$ are spanned as follows:

$$m_t = \sum_{n=1}^{N+1}\sum_{k=1}^{K+1} w_{t,n,k}\,\mu_n, \;\; \bar{\theta}_t = \sum_{n=1}^{N+1}\sum_{k=1}^{K+1} w_{t,n,k}\,\phi_k, \;\; \forall t. \tag{24}$$

Hence, the domain of the bilinear term $m_t\bar{\theta}_t$, which for ease of exposition is denoted by ξ_t, is spanned as follows:

$$\xi_t = \sum_{n=1}^{N+1}\sum_{k=1}^{K+1} w_{t,n,k}\,\mu_n\,\phi_k, \quad \forall t. \tag{25}$$

Let $x_{t,n}$ and be a binary indicator denoting if the n-th interval of variable m_t is active, and $y_{t,k}$ a binary indicator denoting if the k-th interval of variable $\bar{\theta}_t$ is active. The following constraints ensure that only one interval per variable is active:

$$\sum_{n=1}^{N} x_{t,n} = 1, \quad \sum_{k=1}^{K} y_{t,k} = 1, \quad \forall t. \tag{26}$$

Using indicators $x_{t,n}$ and $y_{t,k}$, we ensure that weights $w_{t,n,k}$ that correspond to vertices of non-active intervals are forced to zero as follows:

$$w_{t,n,k} \le x_{t,n-1} + x_{t,n}, \quad n = 2, \ldots, N, \quad k = 1, .., K, \tag{27}$$

$$w_{t,1,k} \le x_{t,1}, \quad w_{t,N+1,k} \le x_{t,N}, \quad k = 1, .., K, \tag{28}$$

$$w_{t,n,k} \le y_{t,k-1} + y_{t,k}, \quad n = 1, \ldots, N, \quad k = 2, \ldots, K, \tag{29}$$

$$w_{t,n,1} \le y_{t,1}, \quad w_{t,n,K+1} \le y_{t,K}, \quad n = 1, \ldots, N. \tag{30}$$

Note that when the two adjoining intervals for a weight are not active, the *rhs* of its corresponding constraints in (27) and (29) will be zero, hence also forcing the *lhs* to zero. Constraints (28) and (30) account for the first and last discretization point. Observe that constraints (26)–(30) enforce adjacency conditions on the weights akin to SOS2 constraints [31]. Overall, (23)–(30) exploit the vertices to have for each domain partition, a convex polyhedral relaxation of the bilinear term — through (23)–(25), and use special ordered sets to have a disjunctive union of these polyhedral relaxations — through (26)–(30).

2) Quadratic Term (m_t^2) in (18): We similarly treat the quadratic term m_t^2 using PPR and the aforementioned partition of variable m_t into N intervals and $(N+1)$ discretization points, yielding a total of $(N+1)\times(N+1)$ vertices. Let $u_{t,n,n'}$ be the weight associated with vertex (n, n'), with

$$\sum_{n=1}^{N+1}\sum_{i=1}^{N+1} u_{t,n,i} = 1, \quad \forall t. \tag{31}$$

The domain of the quadratic term m_t^2, which for ease of exposition is denoted by ζ_t, is spanned as follows:

$$m_t = \sum_{n=1}^{N+1}\sum_{n'=1}^{N+1} u_{t,n,n'}\,\mu_n, \;\; \forall t. \tag{32}$$

$$\zeta_t = \sum_{n=1}^{N+1}\sum_{n'=1}^{N+1} u_{t,n,n'}\,\mu_n\,\mu_{n'}, \quad \forall t. \tag{33}$$

Using the aforementioned indicator $x_{t,n}$, we ensure that weights $u_{t,n,n'}$ that correspond to vertices of non-active intervals are forced to zero as follows:

$$u_{t,n,n'} \le x_{t,n-1} + x_{t,n}, \; n = 2, \ldots, N, \; n' = 1, \ldots, N, \tag{34}$$

$$u_{t,1,n'} \le x_{t,1}, \; u_{t,N+1,n'} \le x_{t,N}, \; n' = 1, \ldots, N, \tag{35}$$

$$u_{t,n,n'} \le x_{t,n'-1} + x_{t,n'}, \; n = 1, \ldots, N, \; n' = 2, \ldots, N, \tag{36}$$

$$u_{t,n,1} \le x_{t,1}, \; u_{t,n,N+1} \le x_{t,N}, \; n = 1, \ldots, N. \tag{37}$$

B. MIQP Problem Summary

Replacing the bilinear term $m_t\bar{\theta}_t$ and the quadratic term m_t^2 by ξ_t and ζ_t, respectively, the NLP problem objective function and constraints are modified as follows.

The objective function term (14b) becomes:

$$p_t = \beta_1\xi_t + \beta_2 m_t + \alpha_2\zeta_t, \quad \forall t. \tag{14b$'$}$$

and similar changes are made in the functional form of J_t in (14e). We refer to this modified objective as (14′).

Constraints (15), (18) and (19) are written as follows:

$$\theta_t = \theta_{t-1} + \gamma_1 m_t + \gamma_2\xi_t + \gamma_3\bar{\theta}_t + \gamma_4\bar{\theta}_t^b + \gamma_{5,t}, \quad \forall t, \tag{38}$$

$$\alpha_1 m_t + \alpha_2\zeta_t - r_t \ge p^{f-}, \quad \forall t, \tag{39}$$

$$\alpha_1 m_t + \alpha_2\zeta_t + r_t \le p^{f+}, \quad \forall t. \tag{40}$$

TABLE I
BUILDING, HVAC AND TEMPERATURE PREFERENCE DATA

Building	
Thermal Resistance of Building Mass, R^b	2×10^{-7} K.h/J
Thermal Resistance of Window, R^w	3.61×10^{-7} K.h/J
Thermal Capacitance of Inside Air, C	6.91×10^{6} J/K
Thermal Capacitance of Building Mass, C^b	1.94×10^{8} J/K
HVAC	
Supply Air Temperature, θ^s	17°C
Valve Position, δ	0.8
Supply Air Flow Rate, m_t	1–6 kg/s
Fan parameter, α_1	0.234 kJ/kg
Fan parameter, α_2	0.0975 (kJ.s)/kg^2
Coefficient of Performance of Coil, η	3.07
Preferences	
Temperature Set-point, $\hat{\theta}_t$	25°C
Low-Occupancy Hours	*(8pm–8am)*
Acceptable Temperature Range, (θ_t^-, θ_t^+)	(18°C, 28°C)
Discomfort Penalty Factor, ϵ_t	\$0.014/°C^2
High-Occupancy Hours	*(8am–8pm)*
Acceptable Temperature Range, (θ_t^-, θ_t^+)	(23°C, 27°C)
Discomfort Penalty Factor, ϵ_t	\$0.090/°C^2
Other	
Specific Heat Capacity of Air, c	1 kJ/(kg.K)

Hence, the ISD NLP problem is transformed to an MIQP problem which is summarized below:

$$\begin{aligned} \textbf{MIQP}: \quad & \text{minimize } (14'), \\ & \text{subject to: } (16), (17), (20), (23)\text{–}(40), \end{aligned} \tag{41}$$

with variables m_t, θ_t, θ_t^b, $\bar{\theta}_t$, $\bar{\theta}_t^b$, ξ_t, ζ_t real, r_t, $u_{t,n,n'}$, $w_{t,n,k}$ non-negative, and $x_{t,n}$, $y_{t,k}$ binary.

V. CASE STUDY

In this section, we present a Case Study, which uses an office building on a summer day. In Section V-A, we list the input data. In Section V-B, we present the parameter values in the closed-form expression of the expected IHCs, J_t.

A. Input Data

We consider a medium-sized office building using data from the DOE commercial reference building library [32]. The data for the building and HVAC parameters as well as temperature related preferences is given in Table I. The energy and regulation reserve prices are obtained from the PJM market [13], and the ambient temperature and irradiance (used along with occupancy to calculate heat Q_t) from the National Solar Radiation Database (NSRDB) [33] for a summer day (July 19th, 2017) in New Brunswick, New Jersey; they are shown in Fig. 3. The optimization problems are implemented with YALMIP toolbox in MATLAB [34] on a laptop Intel i $7-6500$ U at 2.5 GHz with 16 GB RAM. The NLP and MIQP formulations are solved using IPOPT 3.12.10 [35], and GUROBI 9.0.1 [36], respectively. For the MIQP formulation, the number of discretization intervals used is $N = 10$ and $K = 4$.

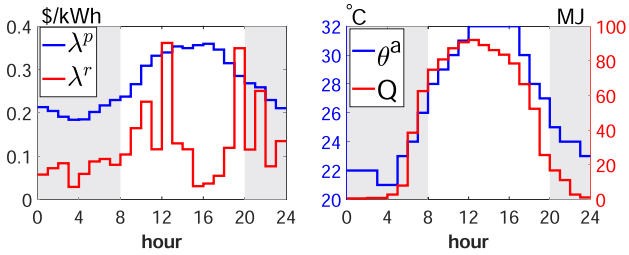

(a) Energy prices λ_t^p; regulation prices λ_t^r.

(b) Ambient Temperature, θ_t^a (left axis); Heat, Q_t (right axis).

Fig. 3. Energy & regulation prices (PJM), and, ambient temperature & heat (NSRDB, new brunswick, NJ), for July 19th, 2017.

TABLE II
NORMALIZED PARAMETER VALUES IN J_t

Parameters	Occupancy (Hours)	
	Low (8pm−8am)	High (8am−8pm)
m^2	–	1.518
$\bar{\theta}_t^2$	–	0.185
$m_t\bar{\theta}_t$	0.412	0.832
r_t	0.031	0.175
m_t	0.036	−1.212
θ_{t-1}	−0.221	−0.587
θ_{t-1}^b	−0.140	−0.146
$\bar{\theta}_t$	0.461	0.548

B. Parameter Values in J_t

In this subsection, we derive the functional form of the expected IHCs, J_t, distinguishing between low and high-occupancy hours. We remind the reader that J_t is a second-degree polynomial in terms of the hourly decision variables, m_t, r_t, and the state variables, $\theta_{t-1}, \theta_{t-1}^b, \bar{\theta}_t$, which captures the regulation signal tracking error and intra-hour incremental occupant discomfort costs.

Table II presents normalized J_t parameters. The costs calculated using these parameters compare well to the actual costs from the pre-processor; R^2 is high (> 0.90), and normalized root-mean-square errors are low ($< 7\%$). Note that a second-degree polynomial is required only for the high-occupancy hours — see values for m_t^2 and $\bar{\theta}_t^2$ in Table II; however, both m_t and $\bar{\theta}_t$ appear in the bilinear term and in linear terms, which renders their interpretation not straightforward. Next, we proceed to some remarks for the parameters in Table II.

First, we observe that the parameters of r_t are positive and their values are larger in high-occupancy hours. Indeed, positive parameters imply that if an HVAC increased the regulation reserve capacity, r_t, the IHCs would increase, because tracking the regulation signal would become more difficult, which would in turn result in higher regulation signal tracking error cost. Larger values in high-occupancy hours are explained by the fact that the stricter temperature bounds limit the HVAC's signal tracking ability.

Second, we observe that if an HVAC increased the supply air flow rate, m_t, the IHCs would increase in low-occupancy hours (positive parameters are associated with terms containing m_t), but would either increase or decrease in high-occupancy

hours (both positive and negative parameters are associated with terms containing m_t). During most of the low-occupancy hours, the ambient temperature θ_t^a and heat Q_t are smaller, thus a higher supply air flow rate would result in intra-hour inside air temperature that would be lower and further away from the preferred set-point, which would in turn result in higher intra-hour incremental occupant discomfort cost. During high-occupancy hours, however, a higher supply air flow rate would move the intra-hour inside air temperature either close to or away from the preferred set-point, depending on the HVAC's hourly operating point, which would in turn result in lower or higher, respectively, intra-hour incremental occupant discomfort cost.

Third, we observe that an increase in the average inside air temperature $\bar{\theta}_t$ would increase the IHCs, with a higher impact during high-occupancy hours (see the $\bar{\theta}_t^2$ term), implying that a higher average inside air temperature would considerably reduce the intra-hour temperature buffer (to the upper bound of the inside air temperature — notably stricter during high-occupancy hours) for performing signal tracking, and would hence increase the IHCs. On the other hand, an increase in the inside air temperature and the building mass temperature at the start of the hour, θ_{t-1} and θ_{t-1}^b, would decrease the IHCs. Collectively, the parameters associated with the temperature terms also account for the intra-hour incremental occupant discomfort cost. For example, if the starting temperatures were higher than the average inside air temperature, it would be possible to maintain the intra-hour temperature closer to the preferred set-point, without compromising signal tracking performance; hence, the actual discomfort incurred during that hour would be less than the average discomfort calculated in (14d), which would in turn result in negative IHCs.

VI. Numerical Results

In this section, we discuss the numerical results for the Case Study. In Section VI-A, we present a base-case using the NLP formulation. In Section VI-B, we compare the NLP and MIQP formulations. In Section VI-D, we analyze the impact of different exogenous factors.

A. Base-Case

In this subsection, we present the solution of the ISD problem, using the NLP formulation, for a base-case that refers to the input data and IHCs parameter values listed in Section V. The decision and state variable trajectories are shown in Fig. 4. The supply air flow rate, m_t (see Fig. 4(a)), rises above its minimum value only during the high-occupancy hours, when the high ambient temperature, θ_t^a, and heat, Q_t, as well as the stricter temperature bounds, (θ_t^-, θ_t^+), and larger discomfort penalty factor, ϵ_t, necessitate larger cooling. The regulation reserve capacity, r_t (see Fig. 4(b)), which is related to m_t through (18) and (19), also takes non-zero values during high-occupancy hours, when it is cost-efficient to do so. The inside air temperature, θ_t (see Fig. 4(c)), is lower and stays further away from the set-point, $\hat{\theta}_t$, during most of the low-occupancy hours; it is higher than the set-point during the high-occupancy (warmer) hours. The building mass temperature, θ_t^b (see Fig. 4(d)), follows a smoother trajectory, due to the large thermal capacitance of the building mass.

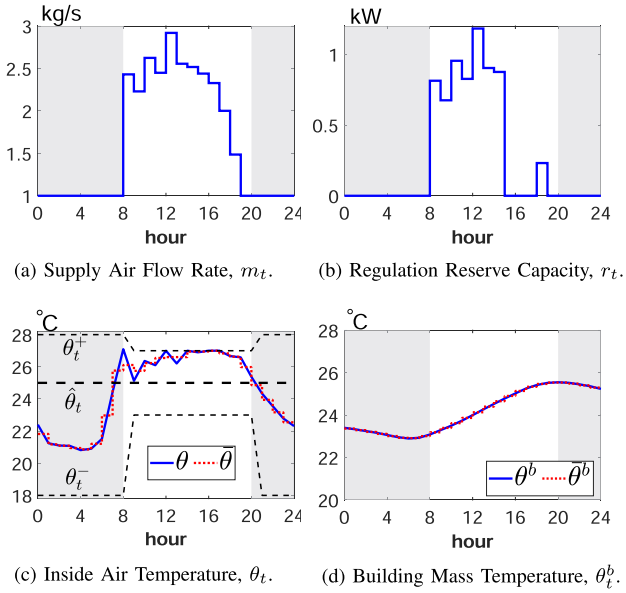

(a) Supply Air Flow Rate, m_t. (b) Regulation Reserve Capacity, r_t.

(c) Inside Air Temperature, θ_t. (d) Building Mass Temperature, θ_t^b.

Fig. 4. Decision and state variables in the base-case.

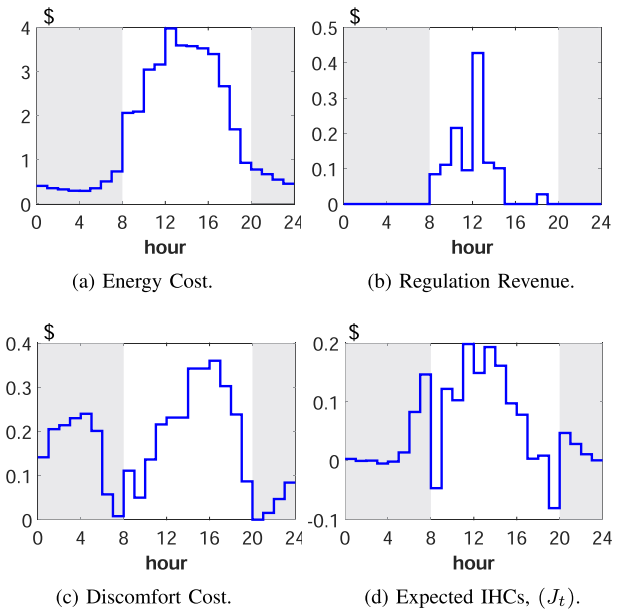

(a) Energy Cost. (b) Regulation Revenue.

(c) Discomfort Cost. (d) Expected IHCs, (J_t).

Fig. 5. Objective function terms in the base-case.

The trajectories for the different objective function terms in (14) are shown in Fig. 5. The energy cost (see Fig. 5(a)) is in general much higher during the high-occupancy hours, due to the higher energy prices and consumption. The regulation revenue (see Fig. 5(b)) is only earned during the high-occupancy hours, when the regulation reserve capacity has been scheduled. The aggregate discomfort cost (see Fig. 5(c)) during the high-occupancy hours is higher compared to the low-occupancy hours, due to the larger penalty factor, ϵ_t, even though the average inside air temperature stays mostly closer to the set-point.

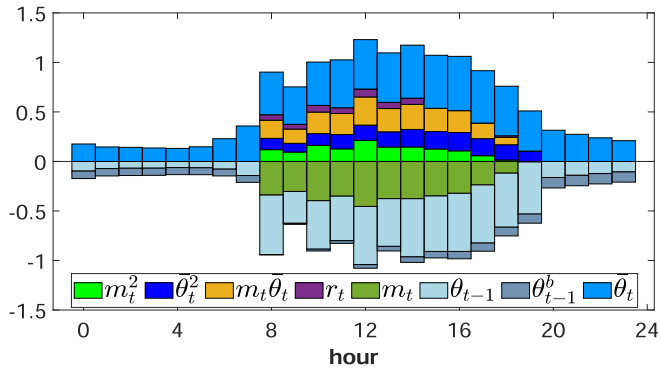

Fig. 6. Breakdown of J_t in the base-case.

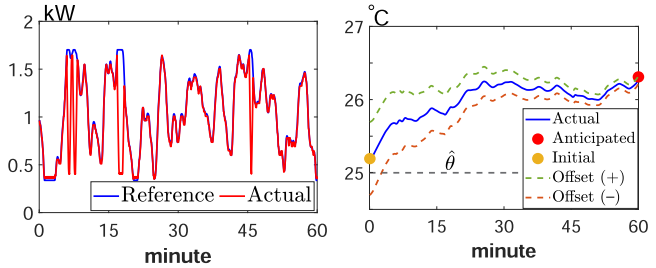

(a) Regulation Signal Tracking. (b) Intra-Hour Temperature.

Fig. 7. Regulation reserve deployment during hour 10.

The expected IHCs (see Fig. 5(d)) takes overall larger values during the high-occupancy hours, when the average inside air temperature, $\bar{\theta}_t$, is close to its upper bound and the offered regulation reserve capacity, r_t, is high (see, e.g., hours $10-15$ in Fig. 4(b) and (c)). When the inside air temperature is decreasing and is further away from the bounds (see, e.g., hours 9 and 20 in Fig. 4(c)), the intra-hour temperature stays much closer to the set-point compared to the average inside air temperature, which results in intra-hour discomfort cost that is lower than the average discomfort calculated in (14d), and hence negative IHCs.

The contribution of different terms towards the expected IHCs, J_t, is shown in Fig. 6. The quadratic terms, m_t^2 and $\bar{\theta}_t^2$, add to the cost during the high-occupancy hours, whereas the cross-term, $m_t\bar{\theta}_t$, does not appear during the low-occupancy hours since the air flow rate, m_t, is at its minimum value (i.e., its normalized value is 0). Likewise, the terms m_t and r_t only appear during the high-occupancy hours (when m_t is above its minimum value). Finally, the temperature terms $\theta_{t-1}, \theta_{t-1}^b$, and $\bar{\theta}_t$ appear during all hours, with their net contribution being larger during the high-occupancy hours.

The regulation reserve deployment, which occurs under the control policy for which the expected IHCs is determined and incorporated into the ISD problem, is presented in Fig. 7. The deployment is shown for hour 10, where it occurs every 4 seconds by modulating the fan power consumption to track the reference regulation signal (Fig. 7(a)). The signal is tracked fairly well and the corresponding inside air temperature change over the hour is the same as the anticipated value (Fig. 7(b)), which is expected due to the symmetric regulation reserve provision and energy-neutral regulation signal. Notably, in Fig. 7(b), we also illustrate two cases where the initial temperature was 0.5^oC lower/higher from the predicted temperature — see offset(+/-). Interestingly, the controller will mitigate this difference, which is reduced to 0.05^oC at the end of the hour.

B. NLP vs. MIQP

In this subsection, we compare the NLP and MIQP formulations, in terms of accuracy and computational performance.

We first consider the base-case, where the NLP and MIQP objective values are 43.681 and 43.666, respectively; their difference is about 0.03%. Notably, the MIQP objective value provides a lower bound (*lb*) to the NLP objective value. An upper bound (*ub*) can be straightforwardly calculated by plugging the MIQP solution into the NLP objective, where m_t is determined using (15) and r_t using (18) and (19). The upper bound is 43.687 (i.e., about 0.013% higher than the NLP objective value). Note the bounds on the objective values are tight since the gaps between the bilinear and quadratic terms ($m_t\bar{\theta}_t$ and m_t^2), and their respective relaxations (ξ_t and ζ_t), are extremely small in the MIQP formulation. The average gap (expressed as percentage of the bilinear/quadratic term) between the bilinear term ($m_t\bar{\theta}_t$) and its relaxation (ξ_t) is 0.02%, whereas between the quadratic term (m_t^2) and its relaxation (ζ_t) is 0.11%. In terms of computational time, the NLP formulation took an order of magnitude more to solve (129 seconds) than the MIQP formulation (11 seconds).

We further compare the NLP and MIQP formulations by perturbing the base-case in terms of the regulation reserve price, ambient temperature and inside air temperature bounds. The considered cases are shown in Table III, where: (i) we scale the regulation reserve price, λ_t^r, by a factor that varies from 0.5 to 5 in increments of 0.5; (ii) we decrease/increase the ambient temperature θ_t^a by a constant value, in steps of 0.5 °C up to 3 °C, and (iii) we modify the inside air temperature bounds (θ_t^-, θ_t^+), in steps of 0.25 °C, up to 1 °C. Table III shows that the average gap (and its standard deviation) between the bilinear/quadratic terms and their relaxations are small (less that 1%), and the bounds on the objective values are extremely tight (the largest difference between the *lb* and *ub* is 0.22%).

In terms of computational time, the results in Fig. 8 indicate that the NLP formulation is highly sensitive to input data and can take significantly longer to solve. For example, if the regulation reserve price λ^r is scaled by 0.5 (case R1) or if the ambient temperature θ^a is decreased/increased by 0.5 °C (cases A1, A2) across all hours, the solution time for the NLP formulation is more than 1 h. On the other hand, the MIQP formulation has a consistent solution time in the order of seconds. Notably, high computational times associated with the NLP formulation are undesirable, especially in a market-based setting, since the HVAC system may be required to solve the ISD problem multiple times before market clearing [37]. We also note that the solution time for the deployment controller was about 3 ms, which is appropriate for the fast few-second deployment of regulation reserve. The pre-processor solves many 3 ms problems, however, this time is not critical as it can be done offline to estimate the parameters of the expected IHCs.

TABLE III
TIGHTNESS OF OBJECTIVE BOUNDS IN DIFFERENT CASES

Case	Parameters	Avg. Gap (std) in (%)		Diff. (%)
		$m_t\bar{\theta}_t$	m_t^2	$\frac{ub-lb}{lb}$
Base	$\lambda_t^r, \theta_t^a, (\theta_t^-, \theta_t^+)$	0.02 (0.04)	0.11 (0.27)	0.05
	Reg. Reserve Price			
R1	$\lambda_t^r \times 0.5$	0.02 (0.03)	0.15 (0.31)	0.05
R2	$\times 1.5$	0.03 (0.05)	0.33 (0.84)	0.07
R3	$\times 2.0$	0.03 (0.06)	0.24 (0.47)	0.06
R4	$\times 2.5$	0.05 (0.06)	0.26 (0.47)	0.10
R5	$\times 3.0$	0.04 (0.06)	0.27 (0.47)	0.10
R6	$\times 3.5$	0.04 (0.06)	0.27 (0.40)	0.12
R7	$\times 4.0$	0.05 (0.06)	0.19 (0.26)	0.17
R8	$\times 4.5$	0.04 (0.06)	0.21 (0.31)	0.18
R9	$\times 5.0$	0.04 (0.06)	0.21 (0.29)	0.22
	Ambient Temperature			
A1	$\theta_t^a - 0.5$	0.03 (0.05)	0.21 (0.38)	0.07
A2	$+0.5$	0.02 (0.04)	0.11 (0.28)	0.04
A3	-1.0	0.04 (0.07)	0.35 (0.63)	0.11
A4	$+1.0$	0.03 (0.06)	0.19 (0.40)	0.06
A5	-1.5	0.06 (0.09)	0.47 (0.88)	0.13
A6	$+1.5$	0.03 (0.05)	0.28 (0.50)	0.08
A7	-2.0	0.07 (0.10)	0.46 (0.77)	0.14
A8	$+2.0$	0.03 (0.06)	0.38 (0.57)	0.11
A9	-2.5	0.06 (0.08)	0.39 (0.57)	0.13
A10	$+2.5$	0.04 (0.06)	0.49 (0.91)	0.12
A11	-3.0	0.05 (0.07)	0.34 (0.56)	0.13
A12	$+3.0$	0.05 (0.07)	0.41 (0.84)	0.11
	Temperature Bounds			
B1	$\theta_t^- - 0.25$, $\theta_t^+ + 0.25$	0.04 (0.07)	0.21 (0.36)	0.08
B2	-0.50, $+0.50$	0.08 (0.10)	0.34 (0.46)	0.14
B3	-0.75, $+0.75$	0.10 (0.13)	0.43 (0.56)	0.16
B4	-1.00, $+1.00$	0.10 (0.14)	0.45 (0.60)	0.16
B5	$+0.25$, -0.25	0.01 (0.04)	0.11 (0.27)	0.04
B6	$+0.50$, -0.50	0.01 (0.02)	0.18 (0.31)	0.06
B7	$+0.75$, -0.75	0.01 (0.01)	0.18 (0.28)	0.06
B8	$+1.00$, -1.00	0.01 (0.03)	0.15 (0.33)	0.04

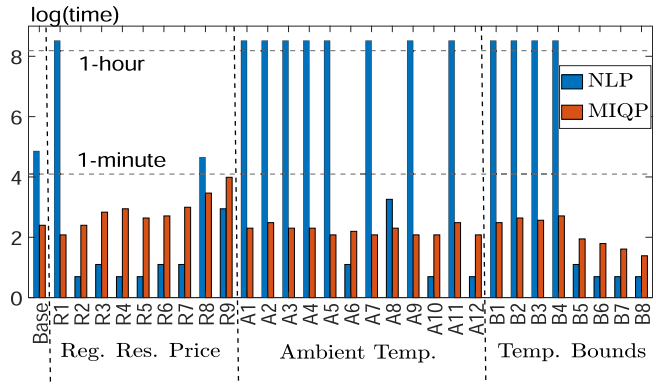

Fig. 8. Computational time in different cases for the NLP and MIQP formulations.

C. Comparison With Existing Approaches

In this subsection, we compare our ISD problem to existing approaches that consider hard constraints, and worst-case-based approaches [9], [10] and [15], which, essentially, consider a worst case deployment of regulation reserve (in either direction) and hard temperature limits, without allowing the HVAC to overbid. A comparison for the Base Case with our approach is shown in Fig. 9. Evidently, [15] leads to conservative estimates for the regulation reserve capacity (Fig. 9(a)), although the differences in the supply air flow rates are small (Fig. 9(b)).

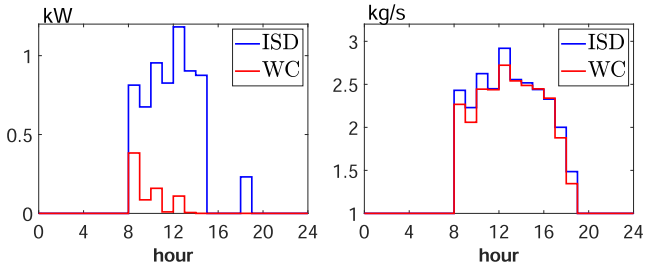

(a) Regulation Reserve Capacity, r_t. (b) Supply Air Flow Rate, m_t.

Fig. 9. Decision variables for the ISD and worst-case (WC) problems in the base-case.

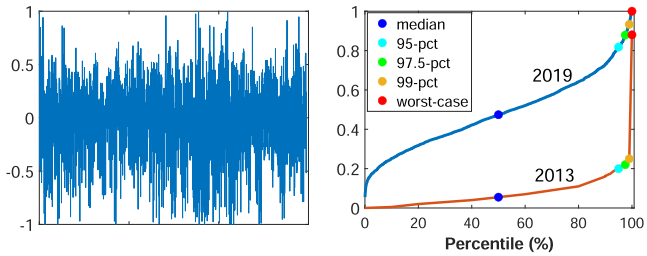

(a) Average Change. (b) Energy Content.

Fig. 10. PJM RegD signal over 15-minute intervals for july, 2019.

The conservativeness can potentially be overcome by offering more capacity than allowed by the HVAC's capability, based on regulation signal statistics. [9] and [10] observe the average change in the signal over 15 minutes to be within 10% and 25% of the capacity, and thus overbid the HVAC capability. However, these numbers were observed using the PJM RegD signal characteristics from 2012 – 2013, which no longer hold. PJM has made significant changes since then. Based on recent data, the potential for overbidding is drastically reduced, and the regulation reserve capacity offers should be much more in line with the HVAC capability. Fig. 10 illustrates the average change over 15-minute intervals for the PJM RegD signal in July 2019 (Fig. 10(a)), and the cumulative distribution of the signal's energy content over 15 minute intervals (Fig. 10). Fig. 10(b) also illustrates the comparison with the data provided [10]. Indicatively, in 2013, the average change requested by RegD over 15 minutes was less than 25% of the regulation capacity with 97.5% probability, whereas in 2019, it was less than 88% of the regulation capacity with the same probability. Notably, 88% was the worst case in [10], which was deemed to be too conservative. Hence, the characteristics of the signal have changed, which do not favor the application of approaches such as [9] and [10] that would still lead to conservative regulation reserve provision.

D. Sensitivity Analysis

In this subsection, we perform sensitivity analysis *w.r.t.* the regulation reserve capacity prices, the ambient temperature, and the inside air temperature bounds.

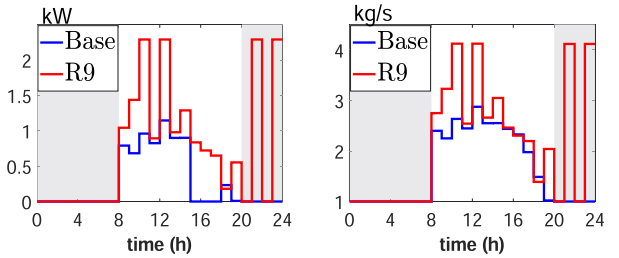

(a) Regulation Reserve Capacity, r_t. (b) Supply Air Flow Rate, m_t.

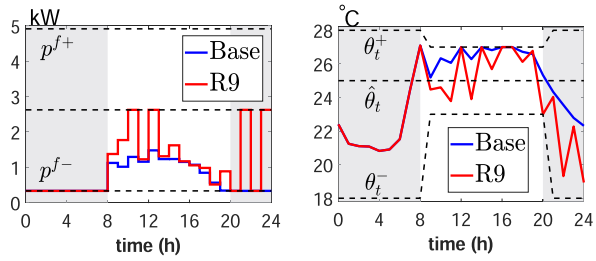

(c) Fan Energy Consumption, p_t^f. (d) Inside Air Temperature, θ_t.

Fig. 11. Impact of regulation reserve prices, λ_t^r.

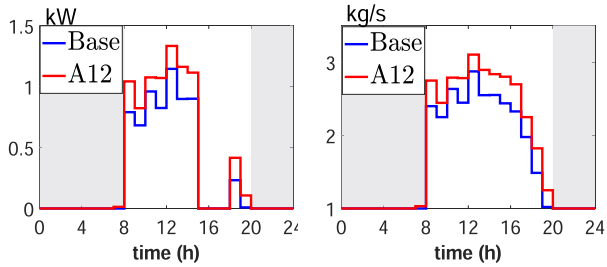

(a) Regulation Reserve Capacity, r_t. (b) Supply Air Flow Rate, m_t.

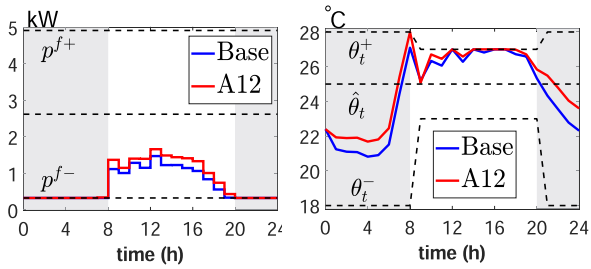

(c) Fan Energy Consumption, p_t^f. (d) Inside Air Temperature, θ_t.

Fig. 12. Impact of ambient temperature, θ_t^a.

1) Regulation Reserve Prices: Fig. 11 compares the base-case with case R9, in which the regulation reserve prices are 5 times higher. Unsurprisingly, case R9 offers, in general, a higher amount of regulation reserve capacity r_t (see Fig. 11(a)). Case R9 also exhibits an increase in the supply air flow rate, m_t (see Fig. 11(b), which follows a pattern that is similar to Fig. 11(a)). Indeed, m_t and r_t are related by (18) and (19), and the capability for offering r_t is maximized when the fan energy consumption, p_t^f, expressed as $\alpha_1 m_t + \alpha_2 m_t^2$, equals the mid-point $(p^{f-} + p^{f+})/2$. For example, see Fig. 11(c), hours $11, 13, 22$, and 24, during which p_t^f is at the mid-point and the HVAC provides the maximum amount of r_t (see Fig. 11(a)). Notably, in the base-case, p_t^f is lower than the mid-point (see Fig. 11(c)), and hence, an increase of m_t (up to the mid-point) in case R9 enables the provision of higher r_t. Evidently, the increase of m_t translates to more cooling and, in general, a lower inside air temperature θ_t (see Fig. 11(d)). Hour 20 (the last high-occupancy hour of the day) is an interesting hour, since θ_t drops to its lower bound, θ_t^-. Taking a closer look, we note that hour 20 has a similar (high) regulation reserve price to hour 13 (see Fig. 11(a)), however, the amount of offered r_t is much lower in hour 20 compared to hour 13. The reason is that if m_t were to increase more in hour 20 (which would enable higher r_t), θ_t would drop below its lower bound (which is not allowed).

2) Ambient Temperature: Fig. 12 compares the base-case with case A12, in which the ambient temperature, θ_t^a, is increased by 3 °C. Evidently, a warmer day would require more cooling, i.e., a higher supply air flow rate, m_t (see Fig. 12(b)), which in turn enables the provision of more regulation reserve capacity, r_t (see Fig. 12(a)). The fan power consumption, p_t^f, increases due to the higher m_t (see Fig. 12(c)), however, since the energy prices dominate the regulation reserve prices, p_t^f increases only to the extent required to keep the inside air temperature θ_t (which is in general elevated compared to the base-case) within the bounds during the high occupancy hours (see Fig. 12(d)).

3) Temperature Bounds: Stricter temperature bounds, (θ_t^-, θ_t^+), require an increase in the supply air flow rate, m_t, to satisfy thermal discomfort preferences during the high-occupancy hours when the inside air temperature, θ_t, is close to the upper bound. Because the HVAC fan operation is in the lower half of its energy consumption, higher m_t due to stricter bounds also leads to higher regulation reserve capacity, r_t. For example, case B8, which has stricter bounds by 1 °C, i.e., $(\theta_t^- + 1, \theta_t^+ - 1)$, results in the provision of about 21% more regulation reserve capacity compared to the base-case.

E. Additional Results

In this subsection, we provide additional numerical results for seven summer days from 2017, which span different values for ambient temperature, irradiance, energy and regulation reserve prices, as shown in Fig. 13.

We estimated the normalized J_t parameter, and calculated the costs which compared well to the actual costs from the pre-processor; average R^2 about 0.90, and normalized root-mean-square errors about 7%. Computational times for the MIQP formulation ranged from 2.2 to 5.0 seconds, indicating a robust performation of the proposed relaxation. The bounds of the relaxation were also tight with the difference between the upper and lower bounds ranging between 0.06% and 0.15%.

The energy consumption and offered regulation reserve capacity are presented in Fig. 14. We make a few interesting observations that illustrate the various factors at play in determining the regulation reserve capacity. For example, July 21st and August 1st are similar days in terms of the cooling requirements

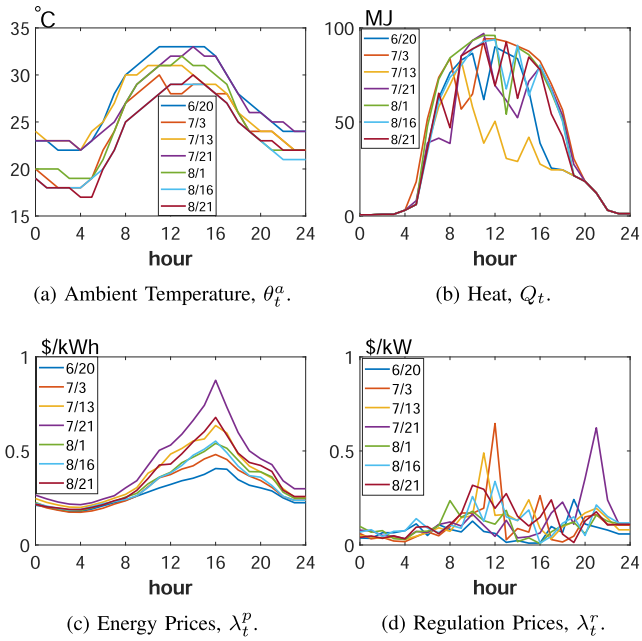

(a) Ambient Temperature, θ_t^a. (b) Heat, Q_t.

(c) Energy Prices, λ_t^p. (d) Regulation Prices, λ_t^r.

Fig. 13. Ambient temperature, irradiance and prices for other representative days.

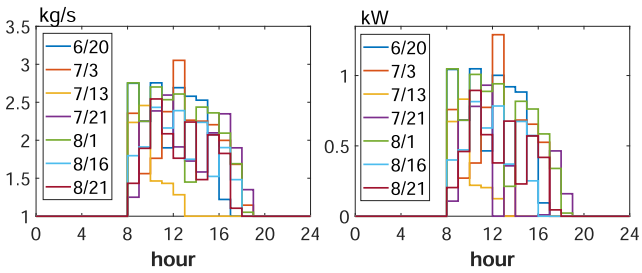

(a) Supply Air Flow Rate, m_t. (b) Regulation Reserve Capacity, r_t.

Fig. 14. Supply air flow rate and regulation reserve capacity for other representative days.

(similar ambient temperatures and heat). However, lower energy prices and relatively higher regulation prices in August 1st result in the HVAC offering significantly more regulation capacity (aggregate 7.3 kW over the entire day compared with 3.5 kW in July 21st). Interestingly, in July 21st, the HVAC is unable to profit from the spike in regulation prices during hour 21 because it is already operating at its minimum fan power consumption. On the other hand, July 3 rd has moderate cooling requirements and relatively smaller energy prices, and hence, it is able to offer the highest regulation capacity observed in single hour during hour 13 profiting from the spike in the regulation reserve price.

VII. Conclusion

In this paper, we considered an integrated scheduling and deployment problem for optimizing the hourly energy consumption and regulation reserve capacity of an HVAC system in a day-ahead market. Our proposal internalized the intra-hour trade-off between regulation signal tracking error and incremental occupant discomfort into the hourly decision-making, by using a pre-processor estimated closed-form representation of the expected intra-hour cost. Computationally efficient piecewise convex relaxations for the complicating non-convex terms in the original NLP problem were also presented, which resulted in an MIQP problem formulation that provided tight bounds for the original NLP problem's objective. We demonstrated the efficacy of our approach, and its relevance pertaining to existing approaches. Next, we plan to present an optimal stochastic formulation for the pre-processor, which will provide detailed characterization of the expected intra-hour cost and optimal intra-hour deployment control policy. Another direction of work will be to quantify the energy consumption and regulation performance of an aggregation of buildings with integrated scheduling and deployment capability (homogeneous/heterogeneous preferences), and to assess the system level impact under wholesale and retail market prices.

References

[1] I. Beil, I. Hiskens, and S. Backhaus, "Frequency regulation from commercial building HVAC demand response," *Proc. IEEE*, vol. 104, no. 4, pp. 745–757, Apr. 2016.

[2] H. Yang et al., "Operational planning of electric vehicles for balancing wind power and load fluctuations in a microgrid," *IEEE Trans. Sustain. Energy*, vol. 8, no. 2, pp. 592–604, Apr. 2017.

[3] J. Wang, S. Huang, D. Wu, and N. Lu, "Operating a commercial building HVAC load as a virtual battery through airflow control," *IEEE Trans. Sustain. Energy*, vol. 12, no. 1, pp. 158–168, Jan. 2020.

[4] E. Vrettos and G. Andersson, "Scheduling and provision of secondary frequency reserves by aggregations of commercial buildings," *IEEE Trans. Sustain. Energy*, vol. 7, no. 2, pp. 850–864, Apr. 2016.

[5] S. A. R. Naqvi, K. Kar, S. Bhattacharya, and V. Chandan, "Peak power minimization for commercial thermostatically controlled loads in multi-unit grid-interactive efficient buildings," *IEEE Trans. Sustain. Energy*, vol. 13, no. 2, pp. 998–1010, Apr. 2022.

[6] G. Chen, H. Zhang, H. Hui, N. Dai, and Y. Song, "Scheduling thermostatically controlled loads to provide regulation capacity based on a learning-based optimal power flow model," *IEEE Trans. Sustain. Energy*, vol. 12, no. 4, pp. 2459–2470, Oct. 2021.

[7] R. de Best, "HVAC industry - Statistics & Facts," 2023. Accessed: Jul. 22, 2022. [Online]. Available: https://www.statista.com/topics/5225/hvac-industry

[8] S. Verbeke and A. Audenaert, "Thermal inertia in buildings: A review of impacts across climate and building use," *Renew. Sustain. Energy Rev.*, vol. 82, pp. 2300–2318, 2018.

[9] Y. Liu, N. Yu, J. Shi, B. Dong, W. Ren, and X. Guan, "Evaluation of frequency regulation provision by commercial building HVAC systems," in *Proc. IEEE 13th Conf. Automat. Sci. Eng.*, 2017, pp. 888–893.

[10] E. Vrettos, E. C. Kara, J. MacDonald, G. Andersson, and D. S. Callaway, "Experimental demonstration of frequency regulation by commercial buildings—part I: Modeling and hierarchical control design," *IEEE Trans. Smart Grid*, vol. 9, no. 4, pp. 3213–3223, Jul. 2018.

[11] E. Vrettos, E. C. Kara, J. MacDonald, G. Andersson, and D. S. Callaway, "Experimental demonstration of frequency regulation by commercial buildings-part II: Results and performance evaluation," *IEEE Trans. Smart Grid*, vol. 9, no. 4, pp. 3224–3234, Jul. 2018.

[12] F. A. Qureshi and C. N. Jones, "Hierarchical control of building HVAC system for ancillary services provision," *Energy Build.*, vol. 169, pp. 216–227, 2018.

[13] PJM, "Markets and operations," 2023. [Online]. Available: https://www.pjm.com/markets-and-operations/

[14] P. Zhao, G. P. Henze, S. Plamp, and V. J. Cushing, "Evaluation of commercial building HVAC systems as frequency regulation providers," *Energy Build.*, vol. 67, pp. 225–235, 2013.

[15] M. Maasoumy, C. Rosenberg, A. S. Vincentelli, and D. S. Callaway, "Model predictive control approach to online computation of demand-side flexibility of commercial buildings HVAC systems for supply following," in *Proc. IEEE Amer. Control Conf.*, 2014, pp. 1082–1089.

[16] D. H. Blum, N. Xu, and L. K. Norford, "A novel multi-market optimization problem for commercial heating, ventilation, and air-conditioning systems providing ancillary services using multi-zone inverse comprehensive room transfer functions," *Sci. Technol. Built Environ.*, vol. 22, no. 6, pp. 783–797, 2016.
[17] L. Fabietti, F. A. Qureshi, T. T. Gorecki, C. Salzmann, and C. N. Jones, "Multi-time scale coordination of complementary resources for the provision of ancillary services," *Appl. Energy*, vol. 229, pp. 1164–1180, 2018.
[18] G. S. Pavlak, G. P. Henze, and V. J. Cushing, "Optimizing commercial building participation in energy and ancillary service markets," *Energy Build.*, vol. 81, pp. 115–126, 2014.
[19] H. Hao, A. Kowli, Y. Lin, P. Barooah, and S. Meyn, "Ancillary service for the grid via control of commercial building HVAC systems," in *Proc. IEEE Amer. Control Conf.*, 2013, pp. 467–472.
[20] Y. Lin, P. Barooah, S. Meyn, and T. Middelkoop, "Experimental evaluation of frequency regulation from commercial building HVAC systems," *IEEE Trans. Smart Grid*, vol. 6, no. 2, pp. 776–783, Mar. 2015.
[21] E. Bilgin, M. C. Caramanis, I. C. Paschalidis, and C. G. Cassandras, "Provision of regulation service by smart buildings," *IEEE Trans. Smart Grid*, vol. 7, no. 3, pp. 1683–1693, May 2016.
[22] F. S. Yanikara, "Decentralized scheduling of EV energy and regulation reserve services in distribution network markets," Ph.D. dissertation, Boston Univ., 2020.
[23] Y. Ma, A. Kelman, A. Daly, and F. Borrelli, "Predictive control for energy efficient buildings with thermal storage: Modeling, simulation, and experiments," *IEEE Control Syst. Mag.*, vol. 32, no. 1, pp. 44–64, Feb. 2012.
[24] K. Sundar, H. Nagarajan, J. Linderoth, S. Wang, and R. Bent, "Piecewise polyhedral formulations for a multilinear term," *Oper. Res. Lett.*, vol. 49, no. 1, pp. 144–149, 2021.
[25] H. Nagarajan, M. Lu, S. Wang, R. Bent, and K. Sundar, "An adaptive, multivariate partitioning algorithm for global optimization of nonconvex programs," *J. Glob. Optim.*, vol. 74, no. 4, pp. 639–675, 2019.
[26] H. C. Van Ness, *Understanding Thermodynamics*. Chelmsford, MA, USA: Courier Corporation, 1983.
[27] ISO-NE, "Transmission, markets, and services tariff: Section III," 2023.
[28] E. Atam and L. Helsen, "Control-oriented thermal modeling of multizone buildings: Methods and issues: Intelligent control of a building system," *IEEE Control Syst. Mag.*, vol. 36, no. 3, pp. 86–111, Jun. 2016.
[29] Y. Yang, G. Hu, and C. J. Spanos, "HVAC energy cost optimization for a multizone building via a decentralized approach," *IEEE Trans. Autom. Sci. Eng.*, vol. 17, no. 4, pp. 1950–1960, Oct. 2020.
[30] NYISO, "Ancillary services manual," 2023.
[31] E. M. L. Beale and J. A. Tomlin, "Special facilities in a general mathematical programming system for non-convex problems using ordered sets of variables," *Oper. Res.*, vol. 69, no. 447/454, 1970, Art. no. 99.
[32] US Department of Energy: Office of Energy Efficiency and Renewable Energy, "Commercial reference buildings," 2023. [Online]. Available: https://www.energy.gov/eere/buildings/commercial-reference-buildings
[33] National Renewable Energy Laboratory (NREL), "National solar radiation database," 2023. [Online]. Available: https://nsrdb.nrel.gov/
[34] J. Löfberg, "YALMIP: A toolbox for modeling and optimization in MATLAB," in *Proc. IEEE Int. Conf. Robot. Automat.*, Taipei, Taiwan, 2004, pp. 284–289.
[35] A. Wächter and L. T. Biegler, "On the implementation of an interior-point filter line-search algorithm for large-scale nonlinear programming," *Math. Prog.*, vol. 106, no. 1, pp. 25–57, Mar. 2006.
[36] Gurobi Optimization, LLC, "Gurobi optimizer reference manual," 2023. [Online]. Available: http://www.gurobi.com
[37] M. Caramanis, E. Ntakou, W. Hogan, A. Chakrabortty, and J. Schoene, "Co-optimization of power and reserves in dynamic T&D power markets with nondispatchable renewable generation and distributed energy resources," *Proc. IEEE*, vol. 104, no. 4, pp. 807–836, Apr. 2016.

Waleed Aslam received the B.S. degree in electrical engineering from the Lahore University of Management Sciences, Lahore, Pakistan, in 2013, and the M.S. degree in electrical and computer engineering from North Carolina State University, Raleigh, NC, USA, in 2017, where he was also a Fulbright Scholar. He is currently working toward the Ph.D. degree in systems engineering with Boston University, Boston, MA, USA. Since December 2022, he has also been an Engineer with Electric Power Research Institute (EPRI), Washington, D.C., USA. His research interests include power system operations, electricity markets, optimization, and control.

Panagiotis Andrianesis (Member, IEEE) is a Graduate with Hellenic Army Academy. He received the B.Sc. degree in economics from the National and Kapodistrian University of Athens, Zografou, Greece, and the Diploma in electrical and computer engineering from the National Technical University of Athens, Athens, Greece, the M.Sc. degree in production management, and the Ph.D. degree in the area of design and analysis of electricity market mechanisms from the University of Thessaly, Volos, Greece. He is currently an Assistant Professor with the Department of Wind and Energy Systems, Technical University of Denmark, Lyngby, Denmark. He was a Research Associate Professor with the Division of Systems Engineering, Boston University, Boston, MA, USA, an Associated Researcher with the Center for Processes, Renewable Energy and Energy Systems (PERSEE), Mines Paris, PSL University, Paris, France, and a Consultant and Research Associate with ECCO International Inc. His research interests include power system economics, electricity markets, operations research, optimization, and applied mathematics. He was the recipient of the 2010 IEEE APS Pre-Doctoral Research Award. Dr. Andrianesis is a Member of INFORMS.

Michael Caramanis (Senior Member, IEEE) received the B.S. degree in chemical engineering from Stanford University, Palo Alto, CA, USA, in 1971, and the M.S. and Ph.D. degrees in engineering from Harvard University, Cambridge, MA, USA, in 1972 and 1976, respectively. Since 1982, he has been with Boston University, Boston, MA, USA, where he is currently a Professor of systems and mechanical engineering. From 2014 to 2008, he chaired the Greek Regulatory Authority for energy and the International Energy Charter's Investment Group, and was personally involved in power market implementations in England from 1989 to 1990 and in Italy from 2000 to 2003. His written work has influenced Power Market design in the U.S. and Europe. He is coauthor of *Spot Pricing of Electricity*, Kluwer, 1987, and has more than 100 refereed publications. His research interests include marginal costing and dynamic pricing on smart Power grids, grid topology control for congestion mitigation, and the extension of power markets to include distribution connected loads, generation, resources. and focuses on mathematical economics, optimization, and stochastic dynamic decision making.